How to cite: Angew. Chem. Int. Ed. 2024, e202400829
doi.org/10.1002/anie.202400829

Ferroptosis

A Ferroptosis-Inducing Arsenene-Iridium Nanoplatform for Synergistic Immunotherapy in Pancreatic Cancer

Xinyang Zhao[+], Xingyun Wang[+], Wei Zhang, Tian Tian, Jingyi Zhang, Jing Wang, Wei Wei, Zijian Guo, Jing Zhao,* and Xiuxiu Wang**

Abstract: Due to multidrug resistance and the high risk of recurrence, effective and less toxic alternative pancreatic cancer treatments are urgently needed. Pancreatic cancer cells are highly resistant to apoptosis but sensitive to ferroptosis. In this study, an innovative nanoplatform (**AsIr@PDA**) was developed by electrostatic adsorption of a cationic iridium complex (**IrFN**) onto two-dimensional (2D) arsenene nanosheets. This nanoplatform exhibits superior ferroptosis-inducing effects with high drug loading capacity and, importantly, excellent anticancer immune activation function, leading to efficient elimination of pancreatic tumors with no observable side effects. Interestingly, **AsIr@PDA** significantly prevents the recurrence of pancreatic cancer in vivo when compared with a cisplatin-loaded nanoplatform. This designed nanoplatform demonstrated superior therapeutic efficacy by synergistic ferroptosis-induced chemotherapy with immunotherapy via an all-in-one strategy, providing new insights for future pancreatic cancer therapy.

Introduction

2D monoelemental nanosheets, such as black phosphorus, bismuthene, and arsenene, have emerged as a new family of nanomaterials with unprecedented advantages and superior performance in biomedicine for their unique physicochemical features.[1] Arsenene, a newly reported 2D monoelemental nanosheet, is composed of arsenic, which is less toxic but possesses excellent therapeutic effects against cancer cells by affecting nuclear DNA replication, nucleotide excision repair, and pyrimidine metabolism pathways by downregulating DNA polymerases.[2] The excellent work on arsenene-based cancer therapy by Tao et al. revealed the great clinical application potential of arsenene.[3] For example, arsenene nanodots effectively reduce the viability of cancer cells, and a significantly lower dosage of an arsenene-based nanomaterial could produce considerable therapeutic efficacy when combined with clinical chemotherapy drugs.[4] Surface-oxidized arsenene nanosheets were reported to catalyze a Fenton-like reaction to generate reactive oxygen species (ROS), and the subsequently engineered arsenene-based nanosheets can serve as an intelligent theranostic platform with active tumor targeting and long-term blood circulation abilities.[5] 2D materials can also be used as ideal drug carriers due to their unique atomic arrangement, high specific surface area, and special electronic properties. For instance, an ingenious loading of β-elemene on 2D arsenene-based nanosheets effectively improved chemo-immunotherapy for cancer treatment.[6] In addition, a newly reported anti-Her2 affibody-decorated arsenene nanosheets overcome drug resistance by inducing ferroptosis in osteosarcoma.[7] Notably, arsenene was discovered to effectively activate direct anticancer immune responses in tumor microenvironment in previous work.[8] In line with the remarkable biocompatibility and immune adjuvant potential, arsenene presents unprecedented totipotency and versatility, endowing arsenene with great clinical application value and prospects.

Pancreatic ductal adenocarcinoma (PDAC) with a Kirsten rat sarcoma viral oncogene homolog (KRAS) mutant is one of the most lethal cancers and highly resistant to apoptosis. The upregulated cysteine-derived metabolite glutathione (GSH) and antioxidant enzymes can detoxify the ROS in PDAC cells, leading to them being insensitive to conventional radiotherapy and chemotherapy.[9] In addition, the multidrug resistance and high risk of recurrence of pancreatic cancer in clinical urgently seek effective and less toxic alternative treatments. Fortunately, studies have revealed that pancreatic cancer is highly sensitive to ferroptosis,[10] a form of non-apoptotic cell death that functions directly or indirectly through different cellular pathways to affect the uptake of cysteine and glutathione, and the synthesis of glutathione peroxidase 4 (GPX4), crippling the cellular antioxidant capacity, producing excess lipid reactive oxygen species, and eventually causing oxidative cell death.[11] Therefore, targeting ferroptosis pathways is becoming a promising approach in the design of effective

[*] X. Zhao,[+] T. Tian, J. Zhang, J. Wang, Prof. Z. Guo, Prof. J. Zhao, X. Wang
Chemistry and Biomedicine Innovation Center (ChemBIC), State Key Laboratory of Coordination Chemistry, School of Chemistry and Chemical Engineering
Nanjing University
Nanjing, 210023, China
E-mail: Jingzhao@nju.edu.cn
wangxiuxiu@nju.edu.cn
X. Wang,[+] W. Zhang, Prof. W. Wei
School of Life Sciences
Nanjing University,
Nanjing, 210023, China
E-mail: weiwei@nju.edu.cn
[+] These authors contributed equally.

nano-agents for pancreatic cancer therapy. In our previous work, we designed and synthesized the mitochondria-targeting iridium complex **IrFN**, which can induce ferroptosis via an autophagy-mediated pathway.[12] Loading metallodrugs onto 2D nanomaterials enables efficient drug delivery and therapeutic efficacy simultaneously and the development of arsenene-based drug-delivery platforms loaded with **IrFN** for cancer therapy is especially exciting.

Herein, we designed an innovative arsenene-iridium nanoplatform by loading cationic **IrFN** on the surface of arsenene to induce more comprehensive ferroptosis. To further enhance the stability and cellular uptake of the platform, a simple polydopamine (PDA) modification was adopted for its superior advantages such as excellent biocompatibility, extraordinary adhesiveness, mild synthesis requirements, and especially the strong photothermal conversion capacity under near-infrared (NIR) irradiation.[13] Importantly, NIR has good tissue penetration and can trigger photodynamic, photothermal, and vibronic-driven action to eradicate cancer cells.[14] In this work, the synthesized nanoplatform **AsIr@PDA** displayed superior ferroptosis-inducing effects with high drug loading capacity and excellent anti-cancer immune activation function, leading to efficient elimination of pancreatic tumors in vivo with high efficacy through ferroptosis-induced chemotherapy, photothermal therapy and immunotherapy (Scheme 1).

Results and Discussion

2D arsenene nanosheets were first synthesized via liquid exfoliation,[2] and the two-dimensional structure is characterized by transmission electron microscopy (TEM) and atomic force microscopy (AFM) in Figure S1. The ferroptosis-inducing metal complex **IrFN** was synthesized by a formerly reported procedure.[12] As a nanosheet with a negatively charged surface, arsenene was combined well with the cationic metallodrug **IrFN** by electrostatic interactions to form **As-IrFN** (AsIr). The factors affecting the biocompatibility and cytotoxicity of materials mainly concentrated on the concentration, shape, number of layers, size, surface charge, and chemical composition. Then, to enhance the stability of the loaded drugs on the arsenene nanosheets, we modified AsIr with PDA to prepare the drug-loaded nanoplatform **AsIr@PDA** (Figure 1a). The **AsIr@PDA** nanoplatform was then characterized by TEM and energy dispersive spectrometry (EDS) analysis (Figures 1b and 1c). As displayed, the PDA wrapped on the surface of the material presented irregular ravines, the entire material was round and spherical and the size was relatively uniform. It was determined through EDS analysis that the elements in **AsIr@PDA** were mainly oxygen, nitrogen, iridium, carbon, and arsenic, corresponding to the characteristics of arsenene-loaded iridium metal drugs externally wrapped with polydopamine (Figure 1c). The average hydrodynamic diameter of **AsIr@PDA** is 289.8 nm as indicated by dynamic light scattering (DLS) analysis (Figure 1d) and particle dispersion index (PDI) is 0.346. As indicated, **AsIr@PDA** can be well dispersed in water in 4 h

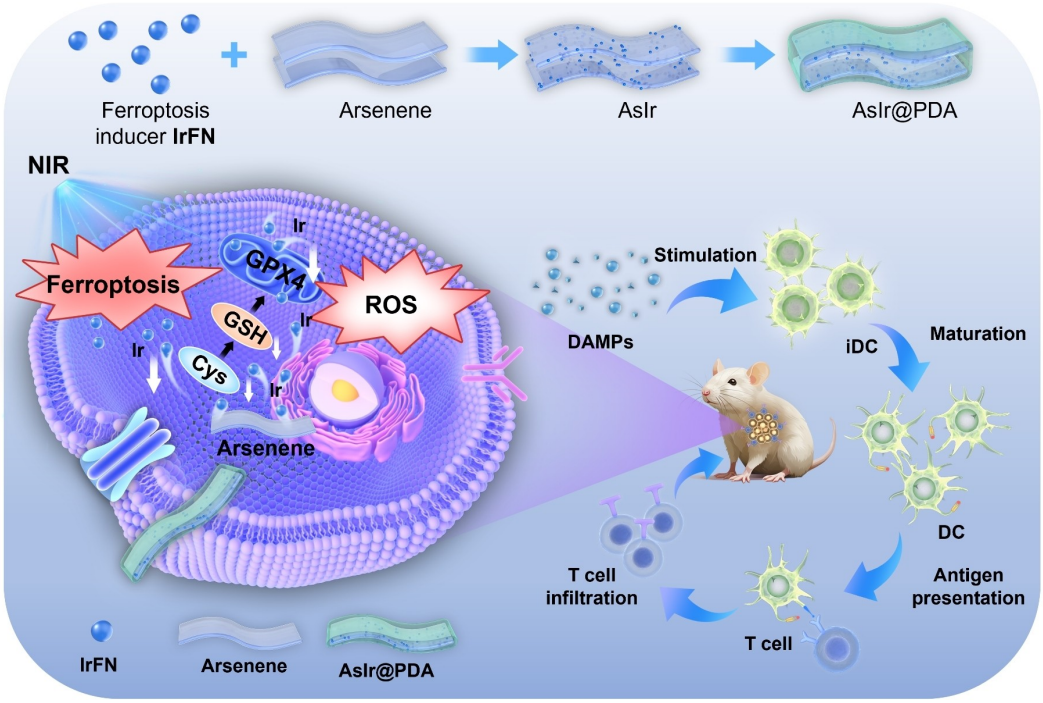

Scheme 1. Schematic illustration of the systemic administration of **AsIr@PDA** for ferroptosis-induced chemotherapy and immunotherapy in pancreatic cancer.

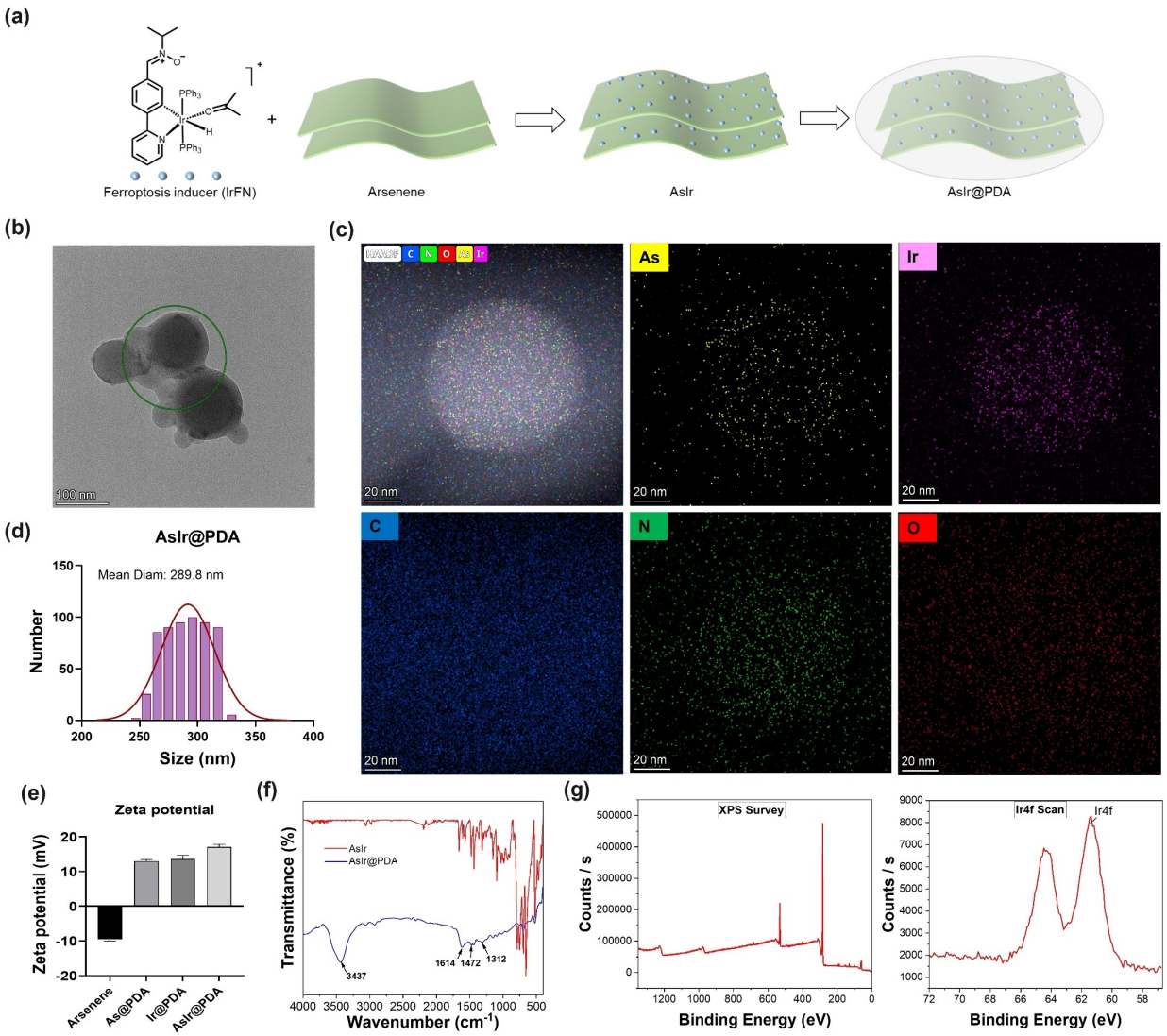

Figure 1. Characterization of **AsIr@PDA**. (a) Preparation of **AsIr@PDA**. (b) TEM images of **AsIr@PDA**; scale bars: 100 nm. (c) Elemental mapping based on TEM images of **AsIr@PDA**; scale bar: 20 nm. (d) DLS analysis of **AsIr@PDA**. (e) Zeta potentials of arsenene, **As@PDA**, **Ir@PDA**, and **AsIr@PDA**. (f) FTIR spectra of AsIr and **AsIr@PDA**. (g) XPS wide-scan survey spectrum of **AsIr@PDA** and XPS analysis of the Ir 4 f spectra. Values are expressed as the mean ± SD of triplicate results.

(Figure S2). Fourier transform infrared (FTIR) spectroscopy is also used to analyze the chemical composition of **AsIr@PDA** after encapsulation (Figure 1f). There is a wide stretching vibration peak near 3437 cm^{-1}, which is due to the presence of O–H and N–H on the PDA. The stretching vibration of C=C in the benzene ring (1614 cm^{-1}), the bending vibration of N–H (1472 cm^{-1}), and the stretching vibration of aliphatic amine C–N (1312 cm^{-1}) also shows the successful coating of PDA. We also conducted a thermogravimetric analysis of the amount of PDA, as shown in Figure S3, the content of PDA in **AsIr@PDA** is 66 w/w%. Through zeta potential measurements, the loaded **IrFN** and modification with PDA transformed the surface charge of the nanomaterial from negative to positive, further confirming successful loading and encapsulation (Figure 1e). Moreover, the loading rate of **IrFN** in **As@PDA** is 920 w/w%, which is calculated by quantifying the amounts of arsenic and iridium by inductively coupled plasma-mass spectrometry (ICP-MS) (Table S1). X-ray photoelectron spectroscopy (XPS) analysis also confirmed the binding energies of arsenic and iridium in **AsIr@PDA** (Figures 1g and S4). The synthesized **AsIr@PDA** successfully allowed the ferroptotic chemotherapy complex **IrFN** to combine with arsenene, which is expected to inhibit tumor proliferation by targeting cancer cells and inducing ferroptosis for pancreatic cancer therapy. To better illustrate the function of the loaded ferroptosis-inducing compound **IrFN**, we also modified arsenene and **IrFN** with PDA to synthesize **As@PDA** and **Ir@PDA** respectively as the control, with the average size of 341.4 nm (PDI: 0.230) and 170.5 nm (PDI: 0.209), respectively (Figure S5).

As PDA possesses strong photothermal conversion capacity,[13a] we next examined the photothermal properties of **AsIr@PDA**. As displayed, the photothermal effect was

both concentration-dependent and light intensity-dependent, and the temperature at the core of the material reached 80 °C after 5 minutes of infrared laser irradiation (808 nm) at an intensity of 1 W/cm^2 (Figures 2a–c). NIR imaging revealed the photothermal effects of arsenene, **As@PDA**, and **AsIr@PDA** all gradually enhanced over time to different degrees. Especially the temperature of **AsIr@PDA** can quickly rise to approximately 80 °C in 3 minutes (Figure 2d). We further investigated the drug release of the contents after irradiation. In both simulated neutral microenvironment (pH 7.4) and tumor microenvironment (pH 6.7), a rapid release of **IrFN** can be observed after NIR irradiation (Figure 2e). Moreover, the degradation of PDA was slow under physiological conditions, while the degradation could be accelerated under acidic conditions, indicating the selective degradation and drug release of **AsIr@PDA** in the tumor microenvironment. To verify the cellular uptake of **IrFN** after being loaded onto arsenene, we quantified the iridium content and found that loading it onto arsenene and further NIR irradiation could significantly increase cellular uptake (Figure 2f). Considering this excellent photothermal therapy (PTT) effect, we then examined the cytotoxicity of **AsIr@PDA** to Pan02 pancreatic cancer cells. The IC_{50} values of **AsIr@PDA** are 1.98 μg/mL and 1.487 μg/mL with NIR irradiation, respectively, better than **As@PDA** (14.79 μg/mL) and **Ir@PDA** (28.01 μg/mL) (Figure S6). To uniform the concentrations and balance the cell viability with all treatments, we then chose 10 μg/mL (based on arsenic) and 17.5 μg/mL (based on iridium) as the standard dosage for the cell experiments (the same As/Ir ratio in **AsIr@PDA**). As shown in Figure 2g, **AsIr@PDA** + NIR for 5 min exhibits the highest cytotoxicity toward Pan02 cells. Importantly, the loading by 2D arsenene endowed **IrFN** with higher tumor accumulation (Figure 2h). Thus, this metal drug loading strategy onto 2D arsenene nanosheets could effectively improve the cancer cell toxicity as well as cancer-targeting ability due to the targeted selectivity and photo-induced releasement of PDA in the slightly acidic tumor microenvironment.

We then investigated the ferroptosis-inducing capabilities of **AsIr@PDA** in Pan02 cells. First, we detected the ability of **AsIr@PDA** to catalyze Fenton-like reactions in vitro. 1,3-Diphenylisobenzofuran (DPBF) and methylene blue (MB) were used to detect the production of ROS. After mixing DPBF or MB with H_2O_2 and **AsIr@PDA**, the changes were determined by UV-Vis absorption. After treatment with different concentrations of **AsIr@PDA** (2.5 μg/mL and 5 μg/mL, based on arsenic content), the

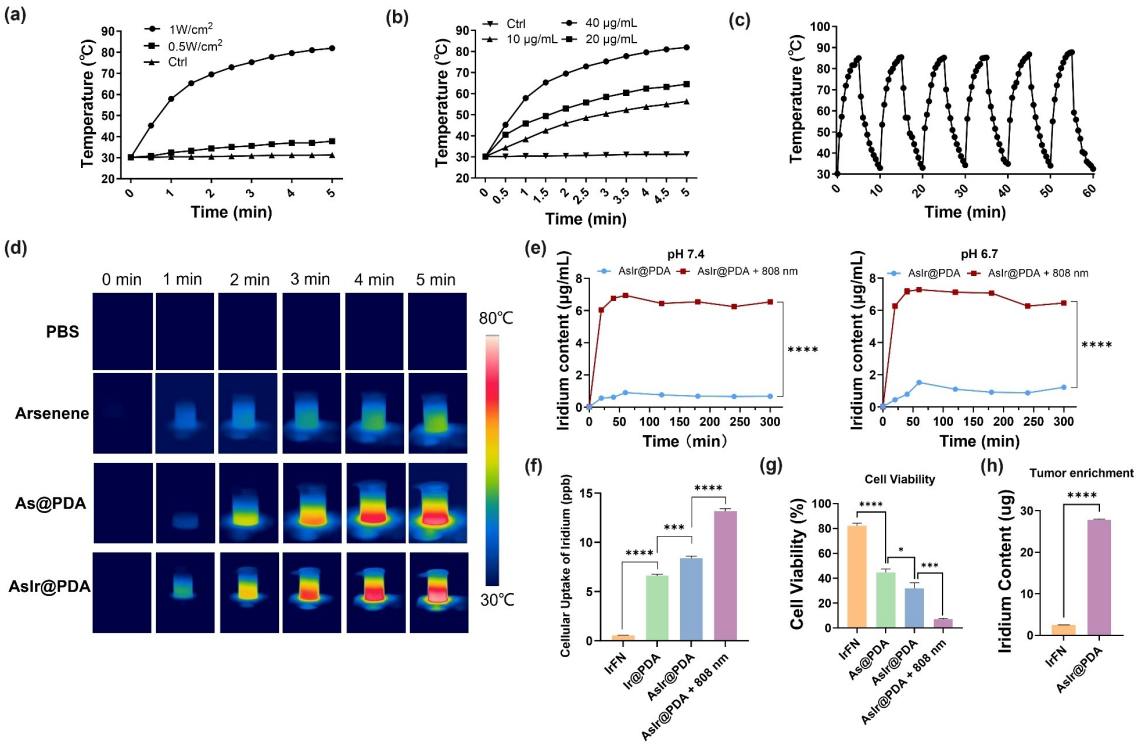

Figure 2. Photoinduced PTT effect, cellular uptake, and cytotoxicity of **AsIr@PDA**. (a) Determination of the photothermal effects of **AsIr@PDA** with different laser intensities under 808 nm irradiation for 5 min. (b) Determination of the photothermal effects of **AsIr@PDA** at different concentrations under 808 nm irradiation (1 W/cm^2) for 5 min. (c) Diagram of the photothermal effect cycle of **AsIr@PDA**. (d) Thermal images of PBS, arsenene, **As@PDA**, and **AsIr@PDA** under 808 nm irradiation (1 W/cm^2) for 5 min. (e) Determination of the amount of iridium released from **AsIr@PDA** in simulated body fluid (pH 7.4) and tumor microenvironment (pH 6.7) with and without irradiation. (f) Cellular uptake of **IrFN**, **Ir@PDA**, **AsIr@PDA**, and **AsIr@PDA** + 808 nm (1 W/cm^2) by Pan02 cells based on Ir content. (g) Cytotoxicity of **IrFN**, **As@PDA**, **AsIr@PDA**, and **AsIr@PDA** + 808 nm (1 W/cm^2) based on arsenic (10 μg/mL) and iridium (17.5 μg/mL) content. (h) Accumulation of **IrFN** in tumor tissues after tail vein injection of **IrFN** and **AsIr@PDA** in Pan02 tumor-bearing mice. Values are expressed as the mean ± SD of triplicate results. Statistical significance was evaluated by t test: *$p < 0.05$, **$p < 0.01$, ***$p < 0.001$, ****$p < 0.0001$.

degradation of DPBF and MB was obvious, indicating that H_2O_2 formed ROS and confirming that **AsIr@PDA** could catalyze a Fenton-like reaction (Figures 3e, 3f, and S7). While no ·OH production could be induced by **AsIr@PDA** through ESR detection, indicating that the formed ROS in vitro are probably $^1O_2$ and $O_2^{\bullet-}$ (Figure S8). Next, we detected the hallmarks of ferroptosis, cellular ROS and lipid ROS. Pan02 cells were treated with PBS, PDA, **As@PDA**, **Ir@PDA**, **AsIr@PDA**, and **AsIr@PDA** + NIR (5 min) for 24 h and then characterized via flow cytometry. As displayed in Figure 3a, **Ir@PDA** stimulated cells to produce slightly more ROS than PDA and **As@PDA**, while **AsIr@PDA** stimulated the highest production of ROS with or without NIR irradiation.

Although as an antioxidant component, PDA was unable to influence the ROS production of **AsIr@PDA** for the burst elevation of ROS mainly induced by the inside arsenene and **IrFN**. **AsIr@PDA** with NIR irradiation also stimulated the highest production of LPO (Figures 3a–d). As the most obvious morphological feature of ferroptosis, the mitochondrial morphology was significantly transformed and the mitochondria shrunk in cells treated with **AsIr@PDA** (Figure 3g) as determined via TEM observations, and the subsequent GPX4 inhibition, system Xc^- inhibition, and GSH depletion also confirmed that ferroptosis was induced by **AsIr@PDA** (Figures 3h–j).

As a 2D inorganic nanomaterial that can effectively activate direct anticancer immune responses, arsenene is also considered a promising candidate nanomedicine for cancer immunotherapy.[8] The overload of ROS induced by arsenene triggers endoplasmic reticulum stress responses to release damage-associated molecular patterns (DAMPs) and "eat-me" signals from dying tumor cells, leading to the activation of antigen-presenting processes to induce subsequent effector tumor-specific $CD8^+$ T-cell immune responses and remodeling of the tumor microenvironment.[8] Therefore, as the drug carrier in this work, the immunomodulatory ability of arsenene confers **AsIr@PDA** with additional immune activation properties. We then detected the release of DAMPs, such as adenosine triphosphate (ATP),

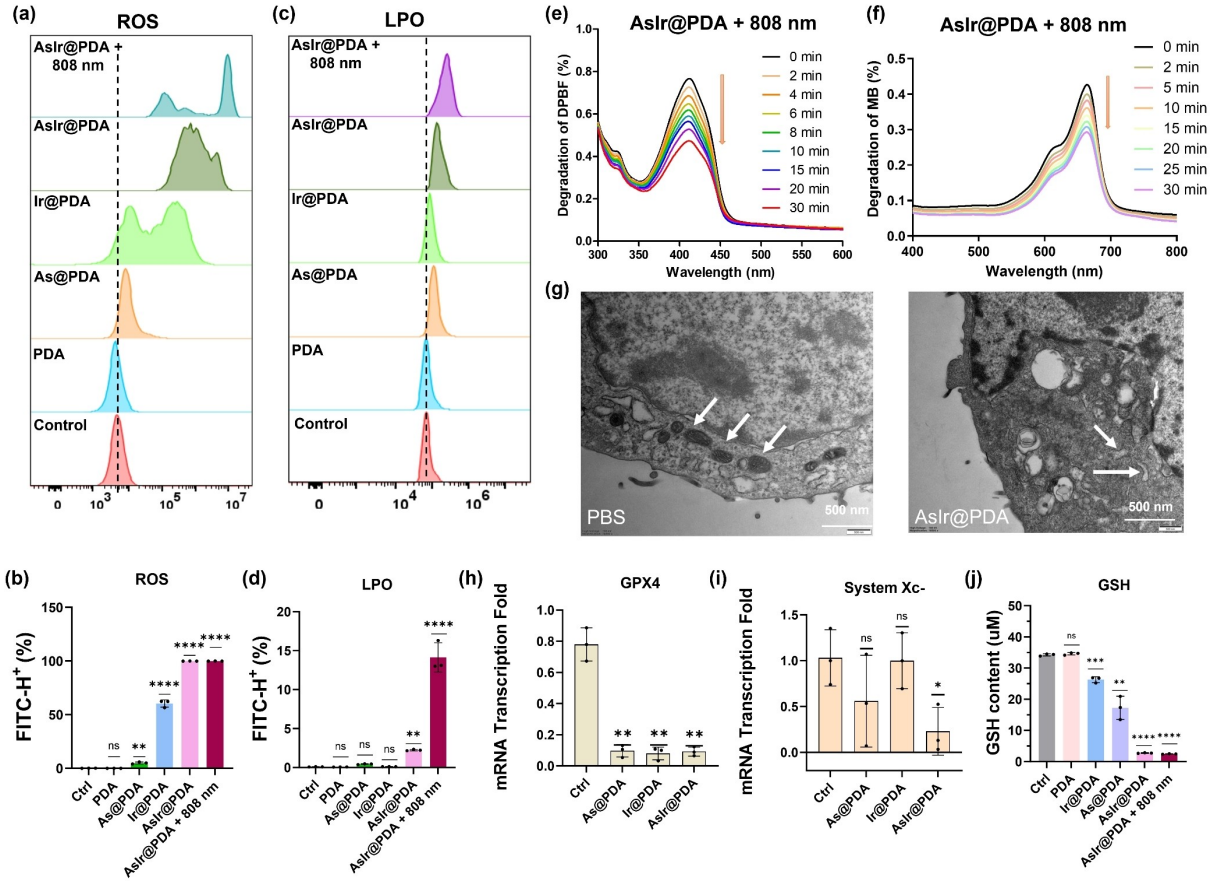

Figure 3. In vitro catalytic Fenton reaction and ferroptosis induced by **AsIr@PDA**. (a) Detection of ROS and LPO production induced by PBS, PDA, **As@PDA**, **Ir@PDA**, **AsIr@PDA**, and **AsIr@PDA** + 808 nm irradiation (5 min) via flow cytometry. (b) Statistical analysis of ROS production from flow cytometry. (c) Detection of LPO production induced by PBS, PDA, **As@PDA**, **Ir@PDA**, **AsIr@PDA**, and **AsIr@PDA** + 808 nm irradiation (5 min) via flow cytometry. (d) Statistical analysis of ROS production from flow cytometry. (e) Detection of DPBF (1 mL, 1 mM) degradation caused by **AsIr@PDA** (5 μg/mL) within 30 min. (f) Detection of MB degradation caused by **AsIr@PDA** (5 μg/mL) within 30 min. (g) TEM images of the morphology of the shrinking mitochondria induced by **AsIr@PDA**; scale bar: 500 nm. (h) mRNA transcriptional folding changes of GPX4 and system X_c^- (i) after treatment with various materials. (j) Changes in GSH content induced by various materials. Values are expressed as the mean ± SD ($n=3$). Statistical significance was evaluated by t test: ns $p \geq 0.05$, *$p < 0.05$, **$p < 0.01$, ***$p < 0.001$, and ****$p < 0.0001$.

high mobility group box 1 protein (HMGB1), and calreticulin (CRT), in Pan02 cells treated with PBS, **As@PDA**, **Ir@PDA**, **AsIr@PDA**, **AsPt@PDA**, and **AsIr@PDA** + NIR. Herein, we synthesized cisplatin-loaded **AsPt@PDA** as a positive control to demonstrate the tolerance of pancreatic cancer cells to apoptosis (Figure S9). As observed by immunofluorescence, HMGB1 translocated from the nucleus, and the "eat me" signal calreticulin was exposed on the cell surface. This phenomenon was much more obvious in the **AsIr@PDA** and **AsIr@PDA** + NIR groups than in the **AsPt@PDA** group. Notably, **As@PDA** and **Ir@PDA** also induced HMGB1 translocation and CRT exposure, but not as strongly as **AsIr@PDA** (Figures 4a–d and S11–12). In addition, the release of ATP was significantly increased in the **AsIr@PDA** and **AsIr@PDA** + NIR treatment groups (Figure 4d). All these results indicated the release of special immunogenic cell death signals after **AsIr@PDA** treatment in Pan02 cells, which is suitable for further investigations of anticancer immune regulation in vivo.

Before the in vivo experiments, we first evaluated the biosafety of **AsIr@PDA** through haematological and biochemical analysis of mouse blood. As illustrated in Figure S13, after intravenous injection of **AsIr@PDA** (As: 80 μg/Kg) for 48 h and 7 d, there were no discernible changes in white blood cells (WBCs), red blood cells (RBCs), haemoglobin (HGB), and platelets (PLTs) values. For the biochemical analysis, the value of alanine transaminase (ALT) increased and creatinine (CRE) decreased after 48 h, while both of them gradually recovered within 7 days. Meanwhile, aspartate transaminase (AST) and blood urea (UREA) values showed a slight increase within a reasonable range over the same period. In addition, blood half-life time of **AsIr@PDA** was also detected, which were 58.5 min and 114.8 min based on iridium and arsenic content, respectively (Figure S14). Then, the antigen presentation process was detected in Pan02 tumor-bearing mice. After the Pan02 tumor models were constructed in female BALB/c mice, the mice were divided into 7 groups and treated with PBS, 808 nm, **As@PDA**, **Ir@PDA**, **AsPt@PDA** or **AsIr@PDA** (with and without irradiation) via tail vein injection. All of the concentrations of **As@PDA**, **Ir@PDA**, or **AsPt@PDA** were dependent on the same dose of arsenic or iridium as those in **AsIr@PDA** (As: 80 μg/Kg, Ir: 140 μg/Kg). The biodistribution of **AsIr@PDA** after 24 h in mice was mainly in the liver and spleen (Figure S15). The markers of antigen presentation processes were then investigated in treated mice after 24 h. CD80 and CD86, two transmembrane glycoproteins, are poorly expressed on most tumor cell membranes. They bind to the receptor CD28 on the surface of T cells to form a double signal and costimulate T lymphocytes to boost the killing of tumors by the immune system.[15] After detecting the expression of CD80 and CD86 in tumor cells under different treatment conditions, the expression of CD80 and CD86 proteins in PBS, 808 nm, **As@PDA**, **Ir@PDA**, and the cisplatin-loaded **AsPt@PDA** group were almost the same and remained at a very low level, facilitating the immune escape of tumor cells. In **AsIr@PDA** groups, the expression of CD80 and CD86 on cell membranes increased significantly. The percentage of mature DCs ($CD86^+/CD80^+$) increased from 4.19 % to

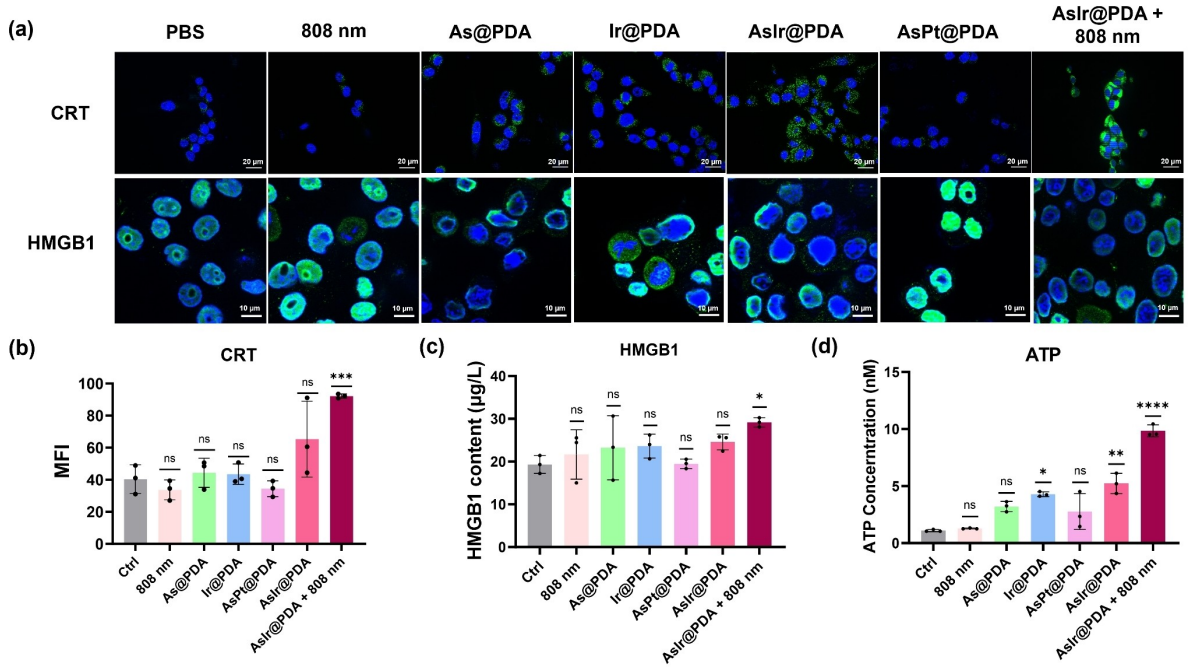

Figure 4. Immunogenic cell death induced by **AsIr@PDA** in Pan02 cells. (a) Calreticulin and HMGB1 merged fluorescence images after Pan02 cells treated with PBS, **As@PDA**, **IrFN**, **AsIr@PDA**, **AsPt@PDA**, and **AsIr@PDA** + 808 nm irradiation (5 min); scale bar: 20 μm (up) and 10 μm (down). (b) Quantitative analysis of the fluorescence of calreticulin. (c) Elisa kit analysis of HMGB1 content after treatment with various materials. (d) Intracellular ATP content after treatment with various materials. Values are expressed as the mean ± SD ($n = 3$). Statistical significance was evaluated by t test: $^*p < 0.05$, $^{**}p < 0.01$, $^{***}p < 0.001$, and $^{****}p < 0.0001$.

27.10 % and 23.31 % without or with 808 nm irradiation (Figures 5a and S16), confirming the potentially effective immune activation of **AsIr@PDA** in vivo.

The immunogenic cell death induced by **AsIr@PDA** can further activate anticancer immune responses in addition to the direct ferroptotic killing of pancreatic cells. Therefore, we detected the production of anticancer immune cells in tumor-bearing mice after treatment for 10 days. After 10 days, tumor-bearing mice were sacrificed, and spleens were separated and prepared as single-cell suspensions for the detection of immune cells by flow cytometry. Significant $CD8^+$ T cell infiltration could be observed in mice spleen after **AsIr@PDA** treatment (with or without irradiation, Figures 5b–c and S17–18), the infiltration of $CD8^+$ T cells and effector $CD8^+$ T cells is higher than in other treatments. Notably, the immune activation effect in the **As@PDA** group was obvious in this pancreatic cancer model, which corresponded with the reported immune activation effect of arsenene nanosheets.[8] Immunofluorescence imaging of $CD8^+$ T cells in mice spleen section also showed that **AsIr@PDA** treatments (with or without irradiation) could significantly increase T cell infiltration (Figure 5d). These results further confirmed the superior immune regulating effect of the **AsIr@PDA** nanoplatform through immunotherapy strategies. Based on the above ferroptosis-inducing and strong ICD anticancer immune activation of **AsIr@PDA** in pancreatic cancer cells, we also investigated the antitumor effect of **AsIr@PDA** in pancreatic tumor-bearing mice. We first detected the antitumor activity of **AsIr@PDA** (with and without irradiation). The tumor volumes and body weights were recorded for 10 days. As displayed in Figure 6, tumor was inhibited most significantly and very importantly, eliminated in all 3 mice by **AsIr@PDA** treatments (with or without irradiation) (Figures 6a and 6b). While there was no significant change in body weight among all mice, indicating the relative biosafety of the **AsIr@PDA** nanoplatform (Figure 6c). It is worth noting that the tumor volume in the **AsPt@PDA** group was significantly inhibited in the first 8 days, while then tumor growth exhibited signs of rebound, and the suppressed tumor began to recur and enlarge (Figures 6a and 6b). This result indicates that apoptosis tolerance and drug resistance might be produced in Pan02 tumors treated by **AsPt@PDA** due to the apoptosis resistance. These results further confirmed the sensitivity of pancreatic cells to ferroptosis, especially **AsIr@PDA**-induced ferroptotic cell death. The synergistic combination of ferroptosis-inducing chemotherapy and anticancer immune activation strategies in a single **AsIr@PDA** platform effec-

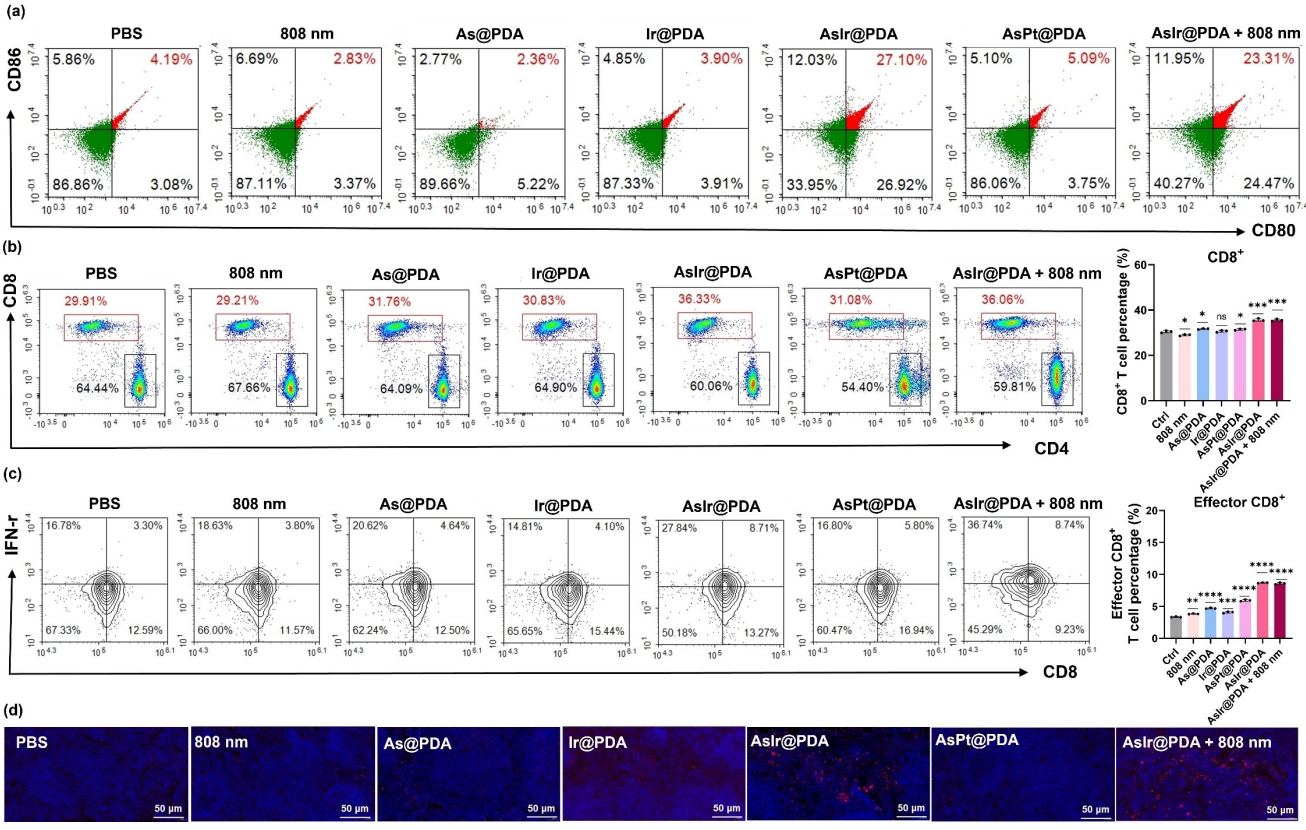

Figure 5. Immune activation induced by **AsIr@PDA** in vivo. (a) Flow cytometry analysis of mature DCs after treatment with PBS, **As@PDA**, **Ir@PDA**, **AsIr@PDA**, **AsPt@PDA**, and **AsIr@PDA** + 808 nm irradiation. (b) Flow cytometry and statistical analysis of $CD8^+$ T cells ($CD3^+$ $CD8^+$ cells) in randomly selected spleen samples. (c) Flow cytometry and statistical analysis of effector $CD8^+$ T cells ($CD3^+$ $CD8^+$ IFN-γ^+ cells) in randomly selected spleen samples. (d) Immunofluorescence imaging of $CD8^+$ T cells in randomly selected spleen samples, scale bar: 50 μm. Values are expressed as the mean ± SD ($n = 3$). Statistical significance was evaluated by One-way ANOVA: ns $p \geq 0.05$, *$p < 0.05$, **$p < 0.01$, ***$p < 0.001$, and ****$p < 0.0001$.

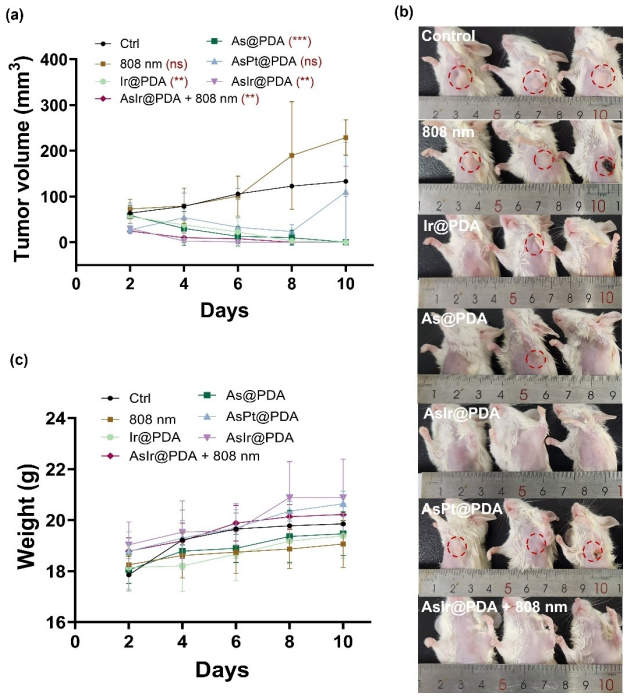

Figure 6. In vivo combined cancer therapeutic effect of **AsIr@PDA**. (a) Tumor volume changes in mice during 10 days of treatment with PBS, 808 nm, **Ir@PDA**, **As@PDA**, **AsIr@PDA**, **AsPt@PDA**, and **AsIr@PDA** + 808 nm. (b) Photos of mice after 10 days of treatment with various materials. (c) Weight changes in mice during 10 days of treatment with various materials. Values are expressed as the mean ± SD ($n=3$). Statistical significance was evaluated by one-way ANOVA; ns $p \geq 0.05$, $^{*}p < 0.05$, $^{**}p < 0.01$, and $^{***}p < 0.001$.

tively prevents the recurrence of tumors and improves the pancreatic cancer treatment effect.

Conclusion

In summary, we designed an innovative arsenene-iridium nanoplatform **AsIr@PDA** by loading ferroptosis-inducing metal complex **IrFN** on arsenene nanosheets and wrapping polydopamine to increase the stability, photothermal effect, and photo-induced drug release. This nanoplatform exhibits superior ferroptosis-inducing capabilities, good photothermal properties, high drug loading capacity, and spatiotemporally controlled drug release, leading to the significant inhibition of pancreatic tumor growth with no observable side effects, thus addressing several key limitations of cancer nanomedicines. The intracellular behavior of the **AsIr@PDA** nanoplatform in pancreatic cancer was also revealed. First, the loaded **IrFN** in **AsIr@PDA** nanoplatform can be released in the acidic tumor microenvironment due to the degradation of PDA. Then the released **IrFN** induces ferroptosis by inhibiting GPX4, system xc^- transport, and the formation of GSH in pancreatic cancer cells with high lethality. In addition to the direct chemotherapeutic ferroptosis, the immunomodulatory property of arsenene endows **AsIr@PDA** with strong immunogenic cell death efficiency and ferroptosis further enhances the significant anticancer immune responses in tumor-bearing mice. Importantly, this enhanced immunotherapy effect by **AsIr@PDA** also prevents the recurrence of tumors when compared with cisplatin-loaded **AsPt@PDA**, overcoming the apoptosis resistance and resolving the multidrug resistance that comes along with a high risk of pancreatic cancer recurrence. In this work, the **AsIr@PDA** nanoplatform achieved a superior therapeutic effect by synergistic ferroptosis-induced chemotherapy and immunotherapy via an all-in-one strategy, which provides a powerful reference for the application of 2D arsenene nanomaterials in future cancer immunotherapy.

Acknowledgements

This work was supported by the National Natural Science Foundation of China (22207053, 22025701, 22293052, 22293053, 22204072, and 92353301), the Natural Science Foundation of Jiangsu Province (BK20220764 and BK20232020), the National Key R&D Program of China (2023YFA1508900), and Nanjing Science and Technology Programme (202305003).

Conflict of Interest

The authors declare no conflict of interest.

Data Availability Statement

The data that support the findings of this study are available in the supplementary material of this article.

Keywords: arsenene · iridium · ferroptosis · immunogenic cell death · pancreatic cancer

[1] a) W. Tao, N. Kong, X. Y. Ji, Y. P. Zhang, A. Sharma, J. Ouyang, B. W. Qi, J. Q. Wang, N. Xie, C. Kang, H. Zhang, O. C. Farokhzad, J. S. Kim, *Chem. Soc. Rev.* **2019**, *48*, 2891–2912; b) X. Yu, A. Li, C. Zhao, K. Yang, X. Chen, W. Li, *ACS Nano* **2017**, *11*, 3990–4001; c) W. Tao, X. B. Zhu, X. H. Yu, X. W. Zeng, Q. L. Xiao, X. D. Zhang, X. Y. Ji, X. S. Wang, J. J. Shi, H. Zhang, L. Mei, *Adv. Mater.* **2017**, *29*, 1603276; d) T. Y. Xue, W. Y. Liang, Y. W. Li, Y. H. Sun, Y. J. Xiang, Y. P. Zhang, Z. G. Dai, Y. H. Duo, L. M. Wu, K. Qi, B. N. Shiyananju, L. J. Zhang, X. Q. Cui, H. Zhang, Q. L. Bao, *Nat. Commun.* **2019**, *10*, 28.

[2] X. Wang, Y. Hu, J. Mo, J. Zhang, Z. Wang, W. Wei, H. Li, Y. Xu, J. Ma, J. Zhao, Z. Jin, Z. Guo, *Angew. Chem. Int. Ed.* **2020**, *59*, 5151–5158.

[3] a) W. Tao, N. Kong, X. Ji, Y. Zhang, A. Sharma, J. Ouyang, B. Qi, J. Wang, N. Xie, C. Kang, H. Zhang, O. C. Farokhzad, J. S. Kim, *Chem. Soc. Rev.* **2019**, *48*, 2891–2912; b) C. Liu, J. Shin, S. Son, Y. Choe, N. Farokhzad, Z. Tang, Y. Xiao, N. Kong, T. Xie, J. S. Kim, W. Tao, *Chem. Soc. Rev.* **2021**, *50*, 2260–2279.

[4] C. Liu, S. Sun, Q. Feng, G. Wu, Y. Wu, N. Kong, Z. Yu, J. Yao, X. Zhang, W. Chen, Z. Tang, Y. Xiao, X. Huang, A. Lv,

C. Yao, H. Cheng, A. Wu, T. Xie, W. Tao, *Adv. Mater.* **2021**, e2102054.
[5] N. Kong, H. Zhang, C. Feng, C. Liu, Y. Xiao, X. Zhang, L. Mei, J. S. Kim, W. Tao, X. Ji, *Nat. Commun.* **2021**, *12*, 4777.
[6] W. Chen, Y. J. Li, C. Liu, Y. Kang, D. T. Qin, S. Y. Chen, J. Zhou, H. J. Liu, B. E. Ferdows, D. N. Patel, X. A. Huang, S. Koo, N. Kong, X. Y. Ji, Y. H. Cao, W. Tao, T. Xie, *Angew. Chem. Int. Ed.* **2023**, *62*, e202308413.
[7] P. He, S. L. Xu, Z. H. Miao, Y. K. Que, Y. Chen, S. Li, Q. M. Ma, R. Yang, W. Wei, Z. B. Zha, Y. Hu, *J. Nanobiotechnol.* **2023**, *21*, 203.
[8] X. Wang, J. Zhang, Y. Hu, X. Zhao, Z. Wang, W. Zhang, J. Liang, W. Yu, T. Tian, H. Zhou, J. Li, S. Liu, J. Zhao, Z. Jin, W. Wei, Z. Guo, *ACS Appl. Mater. Interfaces.* **2022**, *14*, 45137–45148.
[9] a) J. Son, C. A. Lyssiotis, H. Q. Ying, X. X. Wang, S. J. Hua, M. Ligorio, R. M. Perera, C. R. Ferrone, E. Mullarky, N. Shyh-Chang, Y. A. Kang, J. B. Fleming, N. Bardeesy, J. M. Asara, M. C. Haigis, R. A. DePinho, L. C. Cantley, A. C. Kimmelman, *Nature* **2013**, *496*, 101–105; b) A. Arlt, S. S. Muerkoster, H. Schafer, *Cancer Lett.* **2013**, *332*, 346–358; c) H. Q. Ying, A. C. Kimmelman, C. A. Lyssiotis, S. J. Hua, G. C. Chu, E. Fletcher-Sananikone, J. W. Locasale, J. Son, H. L. Zhang, J. L. Coloff, H. Y. Yan, W. Wang, S. J. Chen, A. Viale, H. W. Zheng, J. H. Paik, C. Lim, A. R. Guimaraes, E. S. Martin, J. Chang, A. F. Hezel, S. R. Perry, J. Hu, B. Y. Gan, Y. H. Xiao, J. M. Asara, R. Weissleder, Y. A. Wang, L. Chin, L. C. Cantley, R. A. DePinho, *Cell* **2012**, *149*, 656–670; d) G. M. DeNicola, F. A. Karreth, T. J. Humpton, A. Gopinathan, C. Wei, K. Frese, D. Mangal, K. H. Yu, C. J. Yeo, E. S. Calhoun, F. Scrimieri, J. M. Winter, R. H. Hruban, C. Iacobuzio-Donahue, S. E. Kern, I. A. Blair, D. A. Tuveson, *Nature* **2011**, *475*, 106–109.
[10] M. A. Badgley, D. M. Kremer, H. C. Maurer, K. E. DelGiorno, H. J. Lee, V. Purohit, I. R. Sagalovskiy, A. Ma, J. Kapilian, C. E. M. Firl, A. R. Decker, S. A. Sastra, C. F. Palermo, L. R. Andrade, P. Sajjakulnukit, L. Zhang, Z. P. Tolstyka, T. Hirschhorn, C. Lamb, T. Liu, W. Gu, E. S. Seeley, E. Stone, G. Georgiou, U. Manor, A. Iuga, G. M. Wahl, B. R. Stockwell, C. A. Lyssiotis, K. P. Olive, *Science* **2020**, *368*, 85–89.
[11] a) S. J. Dixon, K. M. Lemberg, M. R. Lamprecht, R. Skouta, E. M. Zaitsev, C. E. Gleason, D. N. Patel, A. J. Bauer, A. M. Cantley, W. S. Yang, B. Morrison, 3rd, B. R. Stockwell, *Cell* **2012**, *149*, 1060–1072; b) W. S. Yang, R. SriRamaratnam, M. E. Welsch, K. Shimada, R. Skouta, V. S. Viswanathan, J. H. Cheah, P. A. Clemons, A. F. Shamji, C. B. Clish, L. M. Brown, A. W. Girotti, V. W. Cornish, S. L. Schreiber, B. R. Stockwell, *Cell* **2014**, *156*, 317–331; c) K. Bersuker, J. M. Hendricks, Z. Li, L. Magtanong, B. Ford, P. H. Tang, M. A. Roberts, B. Tong, T. J. Maimone, R. Zoncu, M. C. Bassik, D. K. Nomura, S. J. Dixon, J. A. Olzmann, *Nature* **2019**, *575*, 688–692.
[12] X. X. Wang, F. Chen, J. Y. Zhang, J. X. Sun, X. Y. Zhao, Y. L. Zhu, W. Wei, J. Zhao, Z. J. Guo, *Sci. China Chem.* **2020**, *63*, 65–72.
[13] a) A. Jin, Y. Wang, K. Lin, L. Jiang, *Bioact. Mater.* **2020**, *5*, 522–541; b) X. Zeng, M. Luo, G. Liu, X. Wang, W. Tao, Y. Lin, X. Ji, L. Nie, L. Mei, *Adv. Sci.* **2018**, *5*, 1800510; c) Z. Li, Y. Hu, K. A. Howard, T. Jiang, X. Fan, Z. Miao, Y. Sun, F. Besenbacher, M. Yu, *ACS Nano.* **2016**, *10*, 984–997; d) Y. Liu, K. Ai, L. Lu, *Chem. Rev.* **2014**, *114*, 5057–5115.
[14] C. Ayala-Orozco, D. Galvez-Aranda, A. Corona, J. M. Seminario, R. Rangel, J. N. Myers, J. M. Tour, *Nat. Chem.* **2023**. doi: 10.1038/s41557-023–01383-y.
[15] D. V. Krysko, A. D. Garg, A. Kaczmarek, O. Krysko, P. Agostinis, P. Vandenabeele, *Nat. Rev. Cancer.* **2012**, *12*, 860–875.

Manuscript received: January 12, 2024
Accepted manuscript online: February 13, 2024
Version of record online: February 28, 2024

Research Articles

Ferroptosis

X. Zhao, X. Wang, W. Zhang, T. Tian, J. Zhang, J. Wang, W. Wei,* Z. Guo, J. Zhao,* X. Wang* **e202400829**

A Ferroptosis-Inducing Arsenene-Iridium Nanoplatform for Synergistic Immunotherapy in Pancreatic Cancer

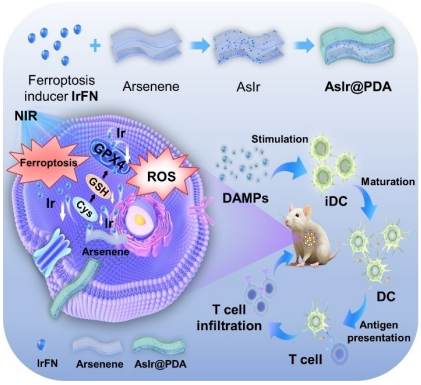

We designed an innovative arsenene-iridium nanoplatform **AsIr@PDA** by loading ferroptosis-inducing metal complex **IrFN** on arsenene nanosheets. The effective release of **IrFN** from **AsIr@PDA** induced pancreatic cancer cell ferroptosis, and the ferroptotic cell death together with the immunomodulatory arsenene endows **AsIr@PDA** with a superior therapeutic effect by synergistic ferroptosis-induced chemotherapy and immunotherapy via an all-in-one strategy.